Unique potentials for the elastic scattering of 350 MeV ^{7}Li from ^{12}C and ^{28}Si

A. Nadasen, J. Brusoe, J. Farhat, T. Stevens, J. Williams, and L. Nieman
University of Michigan, Dearborn, Michigan 48128

J. S. Winfield
National Superconducting Cyclotron Laboratory, Michigan State University, East Lansing, Michigan 48824

R. E. Warner
Oberlin College, Oberlin, Ohio 44075

F. D. Becchetti, J. W. Jänecke, T. Annakkage, J. Bajema, and D. Roberts
University of Michigan, Ann Arbor, Michigan 48109

H. S. Govinden
University of Durban-Westville, Durban, South Africa
(Received 11 May 1995)

Differential cross sections for the elastic scattering of 350 MeV ^{7}Li from ^{12}C and ^{28}Si have been measured. The characteristics of the angular distributions are very similar to those of 318 MeV ^{6}Li scattering from the same targets, with diffractive oscillations at the forward angles and smooth exponential falloff, attributed to the dominance of far-side scattering, at the larger angles. The peak-to-valley ratios of the oscillatory structure are similar to those for ^{6}Li, indicating that the ^{7}Li ground-state quadrupole moment has no discernible effect on the cross sections. Like the ^{6}Li data, the ^{7}Li data define unique phenomenological optical-model potentials. Double-folding model potentials calculated from fundamental nucleon-nucleon interactions also provide reasonably good fits to the experimental data.

PACS number(s): 24.10.Ht, 24.50.+g, 25.70.Bc

I. INTRODUCTION

The elastic scattering of the stable isotopes of Li has been a subject of study for several decades. At very low energies, most of the angular distribution of the differential cross sections is dominated by Coulomb scattering [1]. With increased beam energies, diffractive oscillations emerge [2,3]. These diffractive oscillations are basically sensitive to only the tail of the nuclear potential. Thus for the elastic scattering of both ^{6}Li and ^{7}Li many families of optical potentials were obtained, each providing equally good fit to the data [3].

Recent measurements of 210 and 318 MeV ^{6}Li elastic scattering have provided unique ^{6}Li-nucleus optical-model (OM) potentials [4,5]. The dependence of these potentials on the energy and the target mass has been derived. These unique phenomenological OM potentials have provided a firm basis for the evaluations of folding-model calculations. Thus it was possible to compare directly the potentials generated by the folding calculations with the unique OM potentials before any folding-model cross-section calculation is made. It was found that the folded potentials were similar both in magnitude and shape to the unique OM potentials. Therefore attempts were made to fit the elastic scattering data without any renormalization of these potentials, contrary to the practice at lower energies [3]. Indeed, it was found that the folded potentials satisfactorily reproduced the experimental cross sections.

For ^{7}Li, on the other hand, no unique OM potentials have previously been determined. Data for ^{7}Li elastic scattering were previously available up to a bombarding energy of 132 MeV [6–12]. Several families of ambiguous potentials have been found to provide equally good fits to these data. Thus ^{7}Li-nucleus OM potentials are still plagued with ambiguities which limit our understanding of the ^{7}Li-nucleus interaction.

We have, therefore, embarked on the investigation of ^{7}Li elastic scattering at a higher energy, and report in this paper our measurements of 350 MeV ^{7}Li elastic scattering from ^{12}C and ^{28}Si. Our goal was to determine unique ^{7}Li-nucleus OM potentials, and compare them with the ^{6}Li-nucleus potentials determined previously [5]. We wish to study the effect of the extra neutron in ^{7}Li and to obtain an understanding of the perturbation it produces on the ^{6}Li-nucleus OM potential. The results of this investigation are expected to provide insight into potentials of other neutron-rich projectiles, particularly unstable isotopes such as ^{9}Li and ^{11}Li.

Another interesting feature of ^{7}Li is its large ground-state quadrupole moment [13]. At low energies, this manifests itself in the diffraction region of the elastic scattering angular distribution. It causes the oscillations to be strongly damped, thus reducing the depth of the minima. A comparison of the differential cross sections with those of ^{6}Li should provide an indication of the magnitude of this effect.

Folding-model calculations for ^{7}Li at lower energies have required renormalization of the potentials [6,8,14,15]. Since the present measurements are expected to provide unique

OM potentials, it will be interesting to investigate whether the elastic scattering data can be reproduced without renormalizing the folded potentials. If successful, it will eliminate the problem of renormalization of Li-nucleus potentials, which the nuclear physics community has been trying to understand for decades.

Various aspects of the investigation are outlined in the sections that follow. Section II describes the experimental procedure. Our experimental results are given in Sec. III. Optical-model analyses of the data are presented in Sec. IV. Section V discusses the folding-model calculations. Finally, Sec. VI contains the summary and conclusions.

II. EXPERIMENTAL PROCEDURE

The experiment was performed at the National Superconducting Cyclotron Laboratory (NSCL) at Michigan State University. A high quality 50 MeV/nucleon ^{7}Li beam from the K1200 cyclotron was focused at the center of a 40 cm diameter scattering chamber. The uncertainty in the beam energy was estimated to be $\sim 1\%$ from cyclotron parameters and the A1200 analyzing system. The beam spot on target was typically 1 mm wide by 3 mm high, as observed with a scintillator located on a target ladder at the center of the chamber.

Self-supporting targets of 0.494 and 31 mg/cm^2 natural carbon (99% ^{12}C) and 0.233 and 5.8 mg/cm^2 natural silicon (92% ^{28}Si) were used to make the measurements. In order to optimize the energy resolution, the thin targets were used for most of the measurements. Thick targets were only used for measurements at the large angles where the cross section was low. Overlap data taken with the thin and thick targets permitted correction of errors in the thickness measurements of the thin targets.

The scattered particles were analyzed with a quadrupole-quadrupole-dipole-multipole (QQDM) magnetic spectrometer. The entrance slits to the spectrometer subtended solid angles ranging from 53 to 668 μsr, corresponding to angular acceptance $\Delta\theta$ of 0.185° to 1.48°. The momentum focus was corrected where necessary, in particular when the large angular acceptance was used, by reconstruction of ion trajectories near the nominal focal plane. Although the momentum bite of the spectrometer was large (10% or 70 MeV in energy), the magnetic elements of the spectrometer were continually adjusted to maintain the elastically scattered ^{7}Li particles at the center of the focal plane. This ensured that the data were not subject to efficiency variations across the focal plane.

At the focal plane, two resistive-wire proportional counters provided the horizontal position and trajectory angle of the scattered particles. Two ion chambers gave the vertical position by means of the drift times. The second ion chamber and a stopping plastic scintillator, by serving as ΔE-E counters, provided particle identification. The plastic scintillator also provided the event trigger.

The ΔE-E spectra showed clean separation between ^{7}Li and other particles of the same magnetic rigidity arriving at the focal plane. A window around the ^{7}Li events was used to gate the proportional counter spectrum, thus providing an energy spectrum of ^{7}Li particles. In order to exclude accidental ΔE-E coincidences from adjacent beam bursts, a cyclotron rf timing gate was also employed. The energy spectra had typical energy resolutions of ~ 800 keV. This was sufficient to resolve the ground and first excited states of both targets.

The beam current was measured with two different Faraday cups. For laboratory angles $>6°$, a counter-bored retractable Faraday cup attached to a fixed part of the chamber was used. It subtended an angle of 3°. For the smaller angles, a horizontal plate, moving with the spectrometer and capable of measuring from 2° to 9°, was used. Sufficient overlap data were taken with both cups to check the consistency between the two Faraday cup measurements. All data were written event by event onto magnetic tape for off-line analyses.

During data acquisition, a sample of the data was analyzed on-line in order to monitor dead time, particle identification, position on focal plane, resolution, and statistics. The dead time was monitored by feeding pulses to the focal plane detectors at a rate proportional to the beam current and processing them together with the real events from the detectors. The real data were corrected by assuming the live time to be the ratio of pulser events processed to those fed into the system. The beam current ranged from ~ 1 to ~ 50 nA, depending on the angle of measurement, and it was controlled to keep the dead time below 10% and pileup effects minimal.

The criterion for each datum point was to obtain a statistical accuracy of 2% or a maximum data acquisition time of 30 min. The angular position of the spectrometer could be read to an accuracy of $\pm 0.02°$. After each beamline tune-up, the angular offset of the beam with respect to the spectrometer readout was determined by making small-angle elastic scattering measurements on both sides of the beam axis. The scattering angles were then corrected with any needed offsets.

The angular steps and angular acceptances of the measurements were carefully chosen so that the shape of the angular distribution is well defined. In particular, the narrowest slit ($\Delta\theta = 0.185°$) was used and measurements were made in steps of $\sim 0.25°$ in the diffraction region in order that the depth of the minima are accurately determined. This is necessary to provide information on the effect of the ^{7}Li quadrupole moment. Observations at low energies indicate that this effect tends to fill the minima.

III. EXPERIMENTAL RESULTS

Differential cross sections for the ^{12}C target were measured from 3° to 43° in the center of mass (c.m.). As can be seen in Fig. 1, the data extend over almost eight orders of magnitude. The angular distribution is characterized by limited oscillatory structure at the very forward angles, with no evidence of Rutherford scattering. Beyond about 16° there is a smooth exponential falloff of the cross sections, an indication of the dominance of far-side scattering. It is this region of the angular distribution that is expected to determine the unique OM potentials.

Data for the ^{28}Si target extend from $\sim 3°$ to $\sim 34°$ (c.m.) and cover over seven orders of magnitude (see Fig. 2). This angular distribution is also characterized by forward angle oscillatory structure and smooth exponential falloff at the

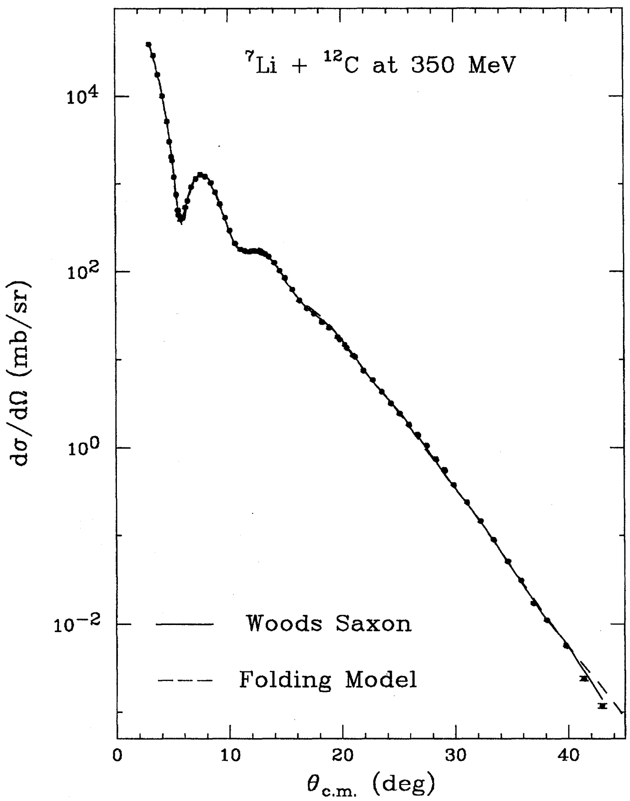

FIG. 1. Angular distribution of the differential cross sections for elastic scattering of 350 MeV ^{7}Li from ^{12}C. The solid line represents the optical-model fit that provides the unique potential parameters listed in Table I. The dashed line represents the folding-model calculations. (See text.)

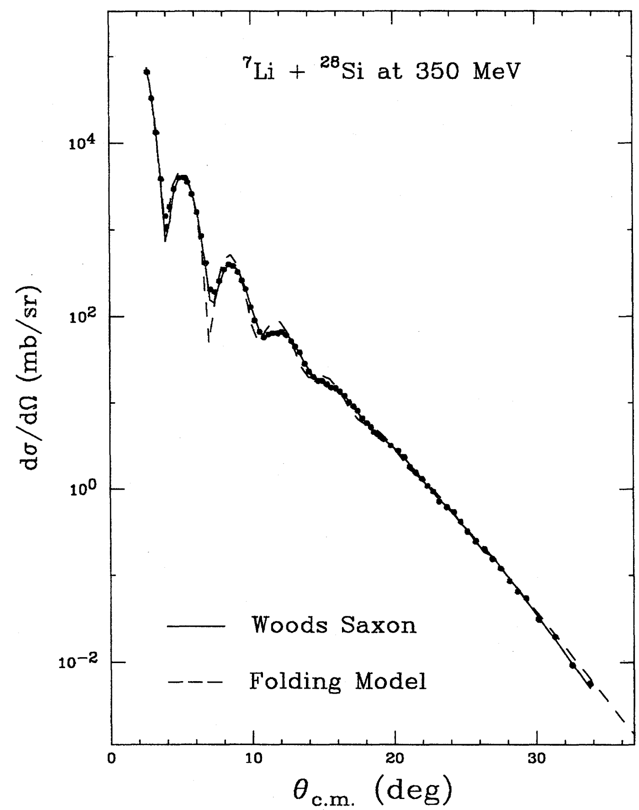

FIG. 2. Same as in Fig. 1, but for ^{28}Si target.

larger angles. The lowest cross section measured for ^{28}Si was 7 μb, while that for ^{12}C was about 1 μb.

The statistical uncertainty of the data was less than 2% for most of the angular range. For cross sections less that 1 mb, slightly larger statistical errors were accepted, but they did not exceed 10%. Combined uncertainties due to dead time corrections, charge integration efficiency, target nonuniformity, and beam spot variation on target were estimated to be 3%. These were added quadratically with the statistical error to obtain the initial relative error. In addition, the uncertainty in effective scattering angle due to uncertainties in angle setting/readout and variations of beam direction during measurements was estimated to be $\pm 0.02°$. This introduced an additional error up to $\sim 8\%$, depending on the slope of the angular distribution, and was folded in quadratically to give the total relative error. The total normalization (systematic) error, due to uncertainties in target thickness, spectrometer solid angle, target angle, and charge integration efficiency, for each angular distribution was estimated to be $\sim 10\%$.

The effect of the quadrupole moment of ^{7}Li on the depth of the diffraction minima was also investigated. In Fig. 3, we plot the cross sections for ^{7}Li on ^{28}Si as a function of momentum transfer (solid dots). Also shown are the cross sections for ^{6}Li+^{28}Si (squares). The data indicate that there is no major difference in the depth of the diffraction minima. Thus it may be concluded that the filling of the minima due to the quadrupole moment of ^{7}Li observed at lower energies does not noticeably manifest itself at this energy, at least within the accuracy of the data.

IV. OPTICAL-MODEL ANALYSIS

The OM analyses of the data were carried out with the code ECIS79 [16]. The conventional nonrelativistic Schrödinger formulation of the elastic potential scattering was employed. Real and volume imaginary central potentials together with a Coulomb potential were included in the analysis. The surface imaginary potential was initially omitted because it provided no improvement in similar analyses of ^{6}Li elastic scattering at about the same energy per nucleon. A spin-orbit potential was not included because no analyzing power data were measured, and the differential cross sections were found to be insensitive to the spin-orbit interaction.

The potential used was

$$U(r)=U_c(r,r_c)-Vf(r,r_0,a_0)-iW_vf(r,r_w,a_w), \quad (1)$$

where $f(r,r_x,a_x)$ is the Woods-Saxon form factor $\{1+\exp[(r-r_xA_t^{1/3})/a_x]\}^{-1}$ and $U_c(r,r_c)$ is the Coulomb potential due to a uniform sphere with charge equal to that of the target nucleus and radius $r_cA_t^{1/3}$.

The search program can be used to carry out searches on any combination of the six parameters in order to minimize χ^2, defined by

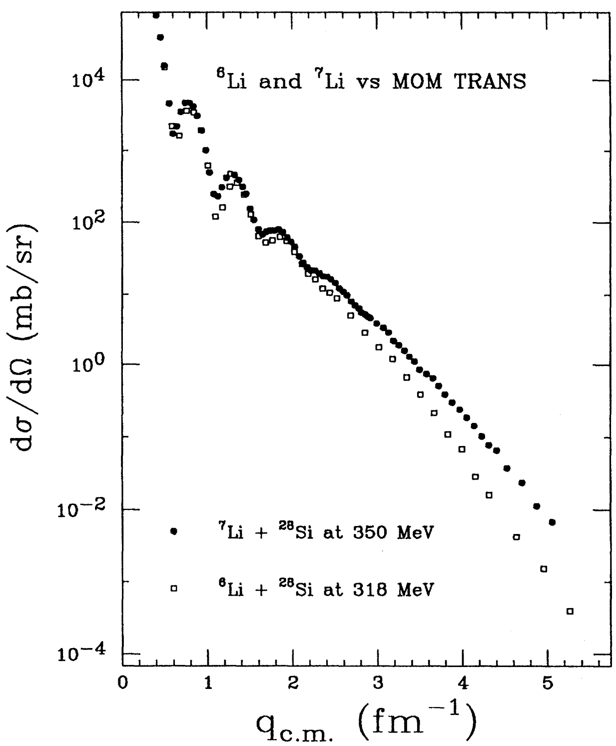

FIG. 3. Differential cross sections for 350 MeV ^{7}Li (circles) and 318 MeV ^{6}Li (squares) elastic scattering from ^{28}Si as a function of momentum transfer.

$$\chi^2=\frac{1}{N}\sum_{i=1}^{N}\left(\frac{\sigma(\theta_i)^{\text{calc}}-\sigma(\theta_i)^{\text{expt}}}{\Delta\sigma(\theta_i)}\right)^2 , \qquad (2)$$

where N is the number of differential-cross-section data points. $\sigma(\theta_i)^{\text{calc}}$ is the ith calculated cross section. $\sigma(\theta_i)^{\text{expt}}$ and $\Delta\sigma(\theta_i)$ are the corresponding experimental cross section and its relative uncertainty, respectively.

Starting parameters were taken from the analyses of 318 MeV ^{6}Li elastic scattering [5]. Initial searches were carried out on various combinations of two parameters. After the lowest χ^2 was reached, three-parameter searches were made. The number of parameters in the searches was monotonically increased until final searches were made on all six parameters. Once reasonably acceptable fits were obtained, the normalization of the data was allowed to vary. No significant improvement to the fit was obtained for either data set with any change in normalization.

To verify that the best possible potentials were obtained, grid searches were also made. Starting with the best values of the six-parameter searches, the real potential was gridded in 5 MeV steps while searching on the other five parameters. Values of V covered in this grid search ranged from 30 to 500 MeV. The resulting χ^2 values for ^{28}Si are shown as the solid line in Fig. 4. Since only a single minimum in χ^2 was obtained, it is concluded that the derived potentials are unique for these data. The corresponding potentials are listed in Table I. The fits to the data are shown as solid lines in Figs. 1 and 2.

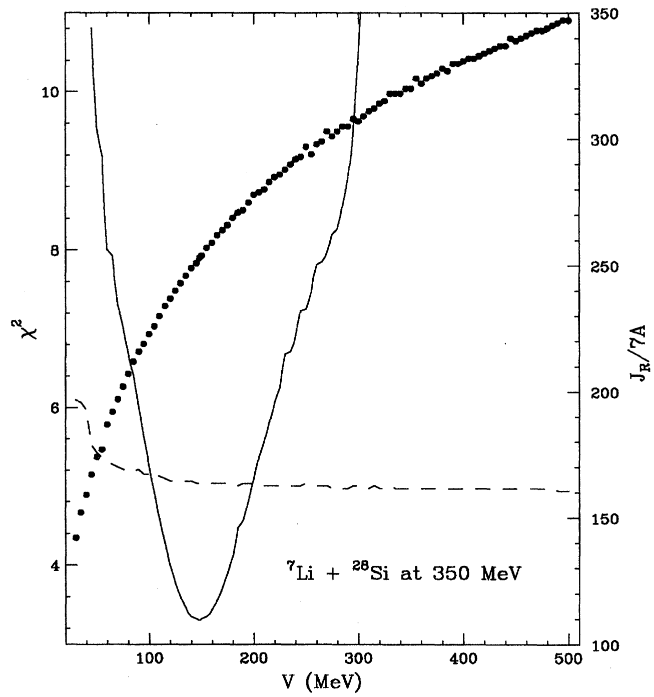

FIG. 4. Variation of χ^2 (left-hand scale) as a function of the strength (V) of the real potential. The solid curve is for the full data set, which selects the unique potential. The dashed curve is for the truncated data set. The circles (right-hand scale) represent the volume integral per nucleon pair ($J_R/7A$).

In an *ad hoc* search for ambiguous families, the angular distribution for the ^{28}Si target was truncated by eliminating the large-angle data. For data truncated to 13° (c.m.), a range of potentials provided acceptable fits. There was no indication of a discrete set of ambiguous potentials. The resulting χ^2 values are shown as the dashed line in Fig. 4. The corresponding volume integrals are indicated by the solid dots. For the ^{12}C truncated data, the χ^2 values also remain constant for values of V from 30 to 500 MeV. These results suggest that any potential fits the truncated data and that the truncated data are not capable of selecting either a unique or discrete ambiguous potential. This is attributed to the fact that the region of oscillatory structure is too limited. If a larger angular range of oscillatory structure existed, the truncated data would be expected to select discrete, ambiguous potentials. The volume integrals of the potentials also do not exhibit the step variations observed in Ref. [4]. They show a smooth monotonic variation from $V=30$ to 500 MeV.

V. FOLDING-MODEL CALCULATIONS

Double-folded potentials for the real part of the ^{7}Li-nucleus interaction were generated using the computer

TABLE I. Unique potential parameters from the OM fit.

	V (MeV)	r (fm)	a_0 (fm)	W_v (MeV)	r_w (fm)	a_w (fm)	$J_R/7A$ (MeV fm^3)	χ^2/N
^{12}C	107.6	1.375	0.854	37.9	1.671	0.758	288	1.0
^{28}Si	147.8	1.228	0.894	50.7	1.519	0.800	257	3.3

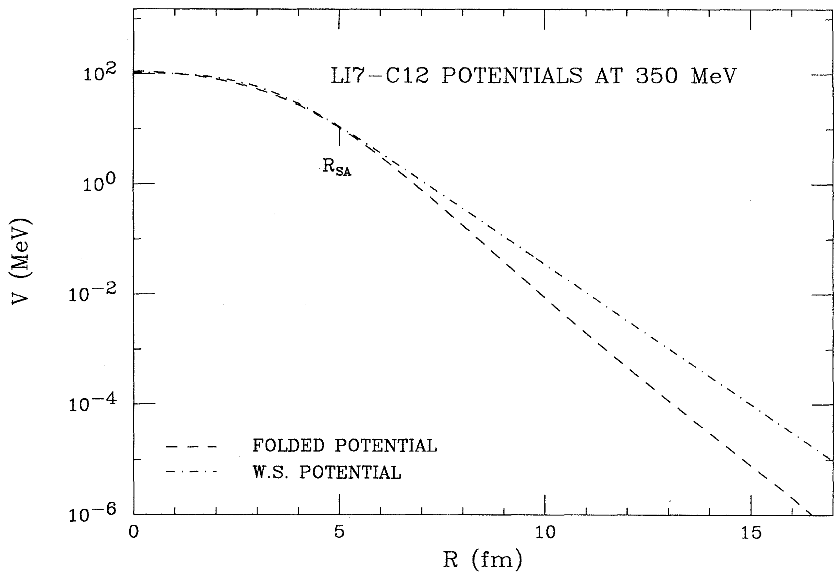

FIG. 5. ^{7}Li+ ^{12}C double-folded real potential (dashed line). The dot-dashed line represents the unique phenomenological OM potential. R_{SA} denotes the strong absorption radius, defined as $kR_{SA}=\eta+\{\eta^2-L_{1/2}(L_{1/2}+1)\}^{1/2}$, where k is the wave number, η is the Sommerfeld parameter, and $L_{1/2}$ is the angular momentum for which the real part of the S matrix is 0.5.

code FOLD [17]. The procedure followed the prescription given by Satchler and Love [18], in which the folded potential can be written as

$$U_F(R)=\int dr_2\int dr_2\rho_1(r_1)\rho_2(r_2)v(r_{12}), \tag{3}$$

where $v(r_{12})$ is the two-body nucleon-nucleon interaction, and ρ_1 and ρ_2 are the distributions of the centers of mass of the nucleons in the ground state of ^{7}Li and ^{12}C or ^{28}Si. The 50 MeV Franey-Love interaction [19] was adopted for the nucleon-nucleon force. Woods-Saxon single-particle wave functions were used to construct the density distributions $\rho_1(r_1)$ or ^{7}Li and $\rho_2(r_2)$ of ^{12}C and ^{28}Si in Eq. (3). The geometry parameters for the Woods-Saxon well were $r_0=1.25$ fm and $a_0=0.65$ fm. The strength V was adjusted to give the known single-particle separation energies.

The calculated potentials were very similar to the phenomenological unique potentials, in terms of both shape and strength. Figure 5 shows the potentials deduced for ^{7}Li + ^{12}C. The dot-dashed line is the empirically determined unique potential, while the dashed line represents the double-folded real potential. The good agreement between the two potentials (up to the strong absorption radius) clearly indicates that the folding-model calculations generate reliable scattering potentials. The large-angle elastic scattering cross sections are obviously most sensitive to this region of the potential. The folded potential for ^{28}Si is slightly deeper than the phenomenological one in the central region.

The folded potentials were used for the real part of the interaction in calculations of 350 MeV ^{7}Li elastic scattering from ^{12}C and ^{28}Si. For the imaginary part a standard volume Woods-Saxon form was adopted. Initial parameters for the imaginary potential were obtained from the phenomenological results. Searches were carried out on these three parameters to optimize the fit to the elastic scattering data. These searches were carried out for different normalizations of the folded potential strength. For the ^{12}C target, optimum fits were obtained for a normalization of $N=1.00$. However, the ^{28}Si data showed a preference for $N=0.86$. The results of the calculations are shown as dashed lines in Figs. 1 and 2. The folding-model calculations seem to reproduce the data almost as well as the phenomenological ones (solid lines in Figs. 1 and 2). There seem to be slight deviations at the largest angles. In the forward angle region for ^{28}Si, the folded potentials seem to predict a stronger diffraction pattern than is observed in the experimental data.

VI. SUMMARY AND CONCLUSIONS

The elastic scattering of 350 MeV ^{7}Li from ^{12}C and ^{28}Si has been investigated. Differential cross sections were measured in fine angular steps with good angular resolution. The data extend to 43° (c.m.) for ^{12}C and 34° (c.m.) for ^{28}Si and they cover over seven orders of magnitude. Diffractive oscillations are only observed over a limited forward angular range of the measurements. Smooth exponential falloffs dominate the angular distributions at the larger angles. The depth of the minima in the diffraction region are very similar to those observed for ^{6}Li elastic scattering at the same energy per nucleon. This is an indication that the effect of the ^{7}Li quadrupole moment on the elastic scattering differential cross sections observed at lower energies does not manifest itself strongly at this energy.

The smooth exponential behavior of the large-angle cross sections is attributed to the dominance of far-side scattering. It is this region of the cross section that is important in determining the unique potentials for the scattering. Unique Woods-Saxon OM potentials for ^{7}Li elastic scattering have been determined for the first time. The volume integrals per nucleon pair obtained for ^{7}Li agree within uncertainties with those found previously for ^{6}Li. The strengths and geometry parameters of the OM potentials are also very similar. This provides verification that the extra neutron exhibits normal behavior and does not cause any unusual perturbation of the Li-nucleus potential such as expected for the neutron halo of ^{11}Li. Truncating the data to the diffraction region does not provide the discrete ambiguous potentials obtained at lower energies, and, in fact, is not effective in selecting any potential.

The double-folded scattering potentials calculated from realistic nucleon-nucleon interactions provide potentials very similar to the unique Woods-Saxon phenomenological OM potentials up to the strong absorption radius. The two potentials are identical for ^{12}C in the interior region of the nucleus. The folded potential reproduces the data as well as the phenomenological potential. The folding calculations overestimate the potential for ^{28}Si which had to be normalized by 0.86 in order to fit the data. This discrepancy is not as yet understood. It seems that folding-model calculations deteriorate with increase in target mass. A similar trend, but to a smaller extent, was previously observed for ^{6}Li.

ACKNOWLEDGMENTS

We wish to thank the cyclotron staff of the National Superconducting Cyclotron Laboratory (NSCL) for the high-quality ^{7}Li beams provided for this experiment. This work was supported in part by the National Science Foundation under Grants No. PHY 9312428 (UM, Dearborn), No. PHY 9122067 (Oberlin College), No. PHY 9214992 (NSCL), and No. PHY 9208468 (UM, Ann Arbor).

[1] K. O. Pheiffer, E. Speth, and K. Bethge, Nucl. Phys. **A206**, 549 (1973); K. Rusek *et al.*, *ibid.* **A407**, 208 (1983); W. Dreves *et al.*, Phys. Lett. **78B**, 36 (1978).
[2] L. T. Chua, F. D. Becchetti, J. Jänecke, and F. L. Milder, Nucl. Phys. **A273**, 243 (1976); C. B. Fulmer *et al.*, *ibid.* **A356**, 235 (1981).
[3] R. Huffman, A. Galonsky, R. Markham, and C. Williamson, Phys. Rev. C **22**, 1522 (1980); P. Schwandt *et al.*, *ibid.* **24**, 1522 (1981).
[4] A. Nadasen *et al.*, Phys. Rev. C **37**, 132 (1988); **39**, 536 (1989).
[5] A. Nadasen *et al.*, Phys. Rev. C **47**, 674 (1993).
[6] J. Cook, M. N. Stephens, and K. W. Kemper, Nucl. Phys. **A466**, 168 (1987).
[7] A. Etchegoyen *et al.*, Phys. Rev. C **38**, 2124 (1988).
[8] G. Tungate *et al.*, J. Phys. G **12**, 1001 (1986).
[9] J. Cook *et al.*, Phys. Rev. C **30**, 1538 (1984).
[10] T. Davinson, V. Rapp, A. C. Schotter, D. Branford, M. A. Nagarajan, I. J. Thompson, and N. E. Sanderson, Phys. Lett. **139B**, 150 (1984).
[11] M. F. Steeden, Jennifer Coopersmith, S. J. Cartwright, M. D. Cohler, N. M. Clarke, and R. J. Griffiths, J. Phys. G **6**, 501 (1980).
[12] K. Katori *et al.*, Nucl. Phys. **A480**, 323 (1988).
[13] K. W. Kerns, Ph.D. thesis, Ohio State University, 1985, available from University Microfilms, Ann Arbor, MI, Order No. 86-03-022; Chem. Phys. Lett. **173**, 157 (1990).
[14] J. Gomez-Camaco, M. Lozano, and M. A. Nagarajan, Phys. Lett. **161B**, 39 (1985).
[15] Y. Sakuragi, M. Kamimura, M. Yahiro, and M. Tranifuji, Phys. Lett. **153B**, 372 (1985).
[16] J. Raynal, Phys. Rev. C **23**, 2571 (1981).
[17] J. Cook and J. A. Carr, Computer Program FOLD, Florida State University, Tallahassee, FL, 1988.
[18] G. R. Satchler and W. G. Love, Phys. Rep. **55**, 183 (1970).
[19] M. A. Franey and W. G. Love, Phys. Rev. C **31**, 488 (1985).